

S-TLLR: STDP-inspired Temporal Local Learning Rule for Spiking Neural Networks

Marco P. E. Apolinario, *Student, IEEE*, and Kaushik Roy, *Fellow, IEEE*,

Abstract—Spiking Neural Networks (SNNs) are biologically plausible models that have been identified as potentially apt for the deployment for energy-efficient intelligence at the edge, particularly for sequential learning tasks. However, training of SNNs poses a significant challenge due to the necessity for precise temporal and spatial credit assignment. Back-propagation through time (BPTT) algorithm, whilst being the most widely used method for addressing these issues, incurs a high computational cost due to its temporal dependency. Moreover, BPTT and its approximations solely utilize causal information derived from the spiking activity to compute the synaptic updates, thus neglecting non-causal relationships. In this work, we propose S-TLLR, a novel three-factor temporal local learning rule inspired by the Spike-Timing Dependent Plasticity (STDP) mechanism, aimed at training SNNs on event-based learning tasks. S-TLLR considers both causal and non-causal relationships between pre and post-synaptic activities, achieving performance comparable to BPTT and enhancing performance relative to methods using only causal information. Furthermore, S-TLLR has low memory and time complexity, which is independent of the number of time steps, rendering it suitable for online learning on low-power devices. To demonstrate the scalability of our proposed method, we have conducted extensive evaluations on event-based datasets spanning a wide range of applications, such as image and gesture recognition, audio classification, and optical flow estimation. In all the experiments, S-TLLR achieved high accuracy with a reduction in the number of computations between $1.1 - 10\times$.

Index Terms—Local learning, Spiking Neural Networks, Memory-efficient learning, STDP.

I. INTRODUCTION

OVER the past decade, the field of artificial intelligence has undergone a remarkable transformation, driven by a prevalent trend of continuously increasing the size and complexity of neural network models. While this approach has yielded remarkable advancements in various cognitive tasks [1], [2], it has come at a significant cost: AI systems now demand substantial energy and computational resources. This inherent drawback becomes increasingly apparent when comparing the energy efficiency of current AI systems with the remarkable efficiency exhibited by the human brain [3]–[6]. Motivated by this observation, the research community has shown a growing interest in brain-inspired computing. The idea behind this approach is to mimic key features of biological neurons, such as spike-based communication, sparsity, and spatio-temporal processing.

All authors are with the Elmore Family School of Electrical and Computer Engineering, Purdue University, West Lafayette, IN, 47907.

Corresponding author: M. P. E. Apolinario, mapolina@purdue.edu

This work has been submitted to the IEEE for possible publication. Copyright may be transferred without notice, after which this version may no longer be accessible.

Bio-plausible Spiking Neural Network (SNN) models have emerged as a promising avenue in this direction. SNNs have already demonstrated their ability to achieve competitive performance compared to more traditional Artificial Neural Networks (ANNs) while significantly reducing energy consumption per inference when deployed in the right hardware [3], [5], [7]–[9]. One of the main advantages of SNNs lies in their event-driven binary sparse computation and temporal processing based on membrane potential integration. These features make SNNs well-suited for deploying energy-efficient intelligence at the edge, particularly for sequential learning tasks [5], [10], [11].

Despite their promise, training SNNs remains challenging due to the necessity of solving precisely temporal and spatial credit assignment problems. While traditional gradient-based learning algorithms, such as backpropagation through time (BPTT), are highly effective, they incur a high computational cost [6], [11], [12]. Specifically, BPTT has memory and time complexity that scales linearly with the number of time steps (T), such as $O(Tn)$ and $O(Tn^2)$, respectively, where n is the number of neurons, making it unsuitable for edge systems where memory and energy are limited. This has motivated several studies that propose learning rules with approximate BPTT gradient computation with limited memory [11]–[16]. However, most of those learning rules have a complexity scaling with the number of synapses, as shown in Table I, which makes them impractical for deep SNN models. Moreover, as most of those learning rules have been derived from BPTT, they only leverage causal information between the pre- and post-synaptic activities, overlooking non-causal information.

To overcome the above limitations, in this paper, we propose S-TLLR, a novel three-factor temporal local learning rule inspired by Spike-Timing Dependent Plasticity (STDP) [17], [18] mechanism. Specifically, S-TLLR is designed to train SNNs on event-based learning tasks while incorporating both causal and non-causal relationships between pre- and post-synaptic activities for updating the synaptic strengths. This feature is inspired by the STDP mechanism from which we propose a generalized parametric STDP equation that uses a secondary activation function to compute the post-synaptic activity. Then, we take this equation to compute an instantaneous eligibility trace [19] per synapse modulated by a third factor in the form of a learning signal obtained from the backpropagation of errors through the layers (BP) or by using random feedback connections directly from the output layer to each hidden layer [20]. Notably, S-TLLR exhibits low memory and time complexity, making it well-suited for online learning on resource-constrained devices.

In addition to this, we demonstrate through experimentation that including non-causal information on the learning process results in improved generalization and task performance. Also, we explored S-TLLR in the context of several event-based tasks with different amounts of spatio-temporal information, such as image and gesture recognition, audio classification, and optical flow estimation. For all such tasks, S-TLLR can achieve performance comparable to BPTT and other learning rules, with much less memory and computation requirements.

The main contributions of this work can be summarized as:

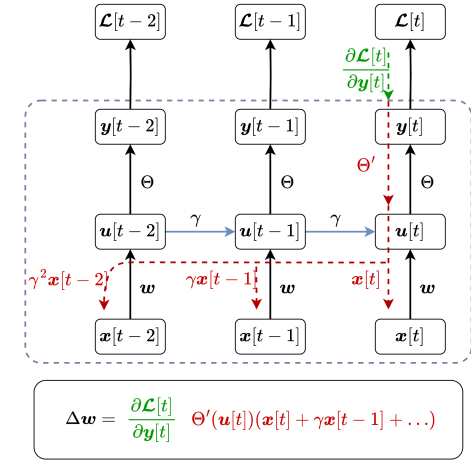
- We introduce a novel temporal local learning rule, S-TLLR, for spiking neural networks, drawing inspiration from the STDP mechanism, while ensuring a memory complexity that scales linearly with the number of neurons and remains constant over time.
- Demonstrate through experimentation the benefits of considering non-causal relationships in the learning process of spiking neural networks, leading to improved generalization and task performance.
- Validate the effectiveness of the proposed learning rule across a diverse range of network topologies, including VGG, U-Net-like, and recurrent architectures.
- Investigate the applicability of S-TLLR in various event-based camera applications, such as image and gesture recognition, audio classification, and optical flow estimation, broadening the scope of its potential uses.

II. RELATED WORK

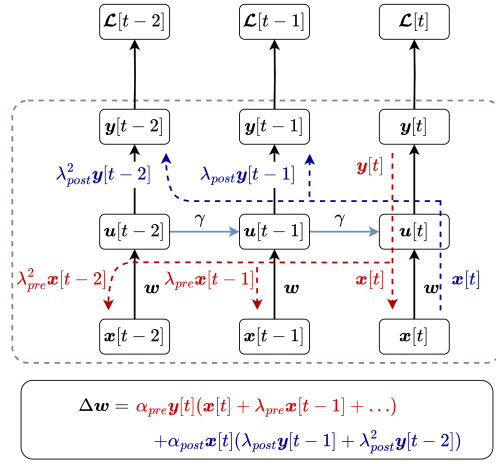
A. Existing methods for training SNNs

Several approaches to training SNNs have been proposed in the literature. These approaches can be classified into four categories: ANN-to-SNN conversion [8], [21], surrogate gradients [9], bio-inspired learning rules [11], [22]–[24], and hybrid methods [25], [26]. The ANN-to-SNN conversion methods involve mapping the weights of a pre-trained artificial neural network (ANN) into an SNN, followed by fine-tuning the thresholds of the spiking neurons to ensure that the mean firing rate of spiking neurons matches the value of their analog counterpart. The main advantage of conversion methods is that they can leverage the well-established training algorithms for ANNs, such as backpropagation, and apply them to SNNs. Such a method has proved to be suitable for training deep SNN models in complex image classification datasets achieving high accuracy [8], [21]. However, such methods can not leverage the inherent temporal information associated with SNNs, and in general, result in models with high latency for inference.

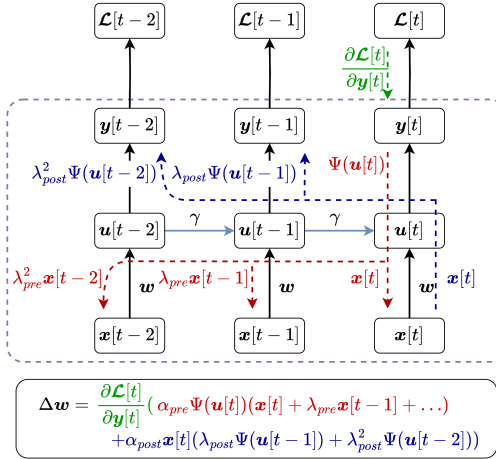
Another approach for training SNNs is based on surrogate gradient methods [9]. These extend the traditional backpropagation through time (BPTT) algorithm to the domain of SNNs. Where the non-differentiable firing function is approximated by a continuous function during the backward pass to allow the propagation of errors. The advantage of these methods is that they can exploit the temporal information of individual spikes so that they can be applied to a broader range of problems than just image classification [27], [28]. Moreover, such methods can result in models with low latency for energy-efficient inference [29]. However, training SNNs based on surrogate



(a) BPTT



(b) STDP



(c) S-TLLR

Fig. 1. Comparison of weight update computation of one spiking layer for (a) BPTT, (b) STDP, and (c) our proposed learning rule S-TLLR. The spiking layer is unrolled over time for the three algorithms while showing the signals involved in the weight updates. The global learning signal is shown in green, while the signals locally available to the layer are inside the dotted box represented as red for the causal term and blue for non-causal terms.

gradients with BPTT incurs high computational and memory costs because BPTT’s requirements scale linearly with the number of time steps. Hence, such methods can not be used for training online under the hardware constraints imposed by edge devices [9].

Researchers have also focused on bio-inspired learning methods based on the principles of synaptic plasticity observed in biological systems, such as spike-timing-dependent plasticity (STDP) [17], [18] or eligibility traces [4], [19], which strengthens or weakens the synaptic connections based on the relative timing of pre- and post-synaptic spikes optionally modulated by a global learning signal. STDP methods are attractive for on-device learning as they do not require any external supervision or error signal. Furthermore, they can adapt to the changing statistics of the input data and exhibit robustness to noise and hardware variability. However, they also have several limitations, such as the need for a large number of training examples and the difficulty of training deep networks or complex ML problems [22]. In contrast, three-factor learning rules using eligibility traces (neuron local synaptic activity) modulated by an error signal, like e-prop [11], can produce more robust learning overcoming limitations of unsupervised methods such as STDP. Nevertheless, typically, such methods’ time and space complexity make them impractical to be used in deep SNNs.

Hybrid approaches combine two or more of the above methods to take advantage of their respective strengths. For example, the conversion of ANNs to SNNs can be followed by spike-based or bio-inspired learning [25]. Similarly, STDP can be combined with backpropagation to achieve faster convergence and better stability, as studied in [26]. These methods can achieve high performance and energy efficiency for on-device learning, but they are often more complex and difficult to optimize than the individual methods. Overall, the choice of the training method depends on the specific application and hardware constraints.

B. Learning rules addressing the temporal dependency problem

As discussed in the previous section, the training methods based on a surrogate gradient using BPTT results in high-performance models. However, their major limitations are associated with high computational requirements that are unsuitable for low-power devices. Such limitations came from the fact that BPTT has to store a copy of all the spiking activity to exploit the temporal dependency of the data during training. In order to address the temporal dependency problem, several methods have been proposed where the computational requirements are time-independent while achieving high performance. For instance, the RTRL [13] algorithm attempts to approximate the gradients computed by BPTT at the cost of storing some intermediate states. Although it has not been originally proposed to be used on SNNs, it could be applied to them by combining with surrogate gradients [9]. More recently, other methods such as e-prop [11], OSTL [12], and OTTT [16], derived from BPTT, allow learning on SNNs using only temporally local information. However, with the

TABLE I
COMPARISON OF S-TLLR WITH LEARNING METHODS FROM THE LITERATURE (WHERE n IS THE NUMBER OF NEURONS AND T TOTAL NUMBER OF TIME STEPS)

Method	Memory — Time Complexity	Temporal Local	Leverage Non-Causality
BPTT	$Tn - Tn^2$	X	X
RTRL [13]	$n^3 - n^4$	✓	X
e-prop [11]	$n^2 - n^2$	✓	X
OSTL [12]	$n^2 - n^2$	✓	X
ETLP [14]	$n^2 - n^2$	✓	X
OSTTP [15]	$n^2 - n^2$	✓	X
OTTT [16]	$n - n^2$	✓	X
S-TLLR (Ours)	$n - n^2$	✓	✓

exception of OTTT, all of these methods have a memory and time complexity, shown in Table I, that makes them impractical for being used on deep SNNs. Moreover, since such methods have been derived as approximations of BPTT, they only use causal relations between pre- and post-synaptic activity, leaving non-causal relations unexplored as those used in STDP shown in Fig. 1.

C. Combining STDP and backpropagation

As previously discussed, STDP has been used to train SNNs models in an unsupervised manner [22]–[24]. However, such approaches suffer from severe drawbacks, such as requiring a high number of timesteps (latency), resulting in low accuracy performance and being unable to scale for deep SNNs. So, to overcome such limitations, there have been some previous efforts to use STDP in combination with backpropagation for training SNNs, by either using STDP followed for fine-tuning with BPTT [26] or modulating STDP with an error signal [30]–[32]. However, such methods either do not address the temporal dependency problem of BPTT or do not scale for deep SNNs or complex computer vision problems.

III. BACKGROUND

This section first describes the leaky-integrate and fire (LIF) neuron model used in this work. Then the Synaptic Time-Dependent Plasticity (STDP) mechanism is presented as an unsupervised mechanism used for training SNNs. Finally, the relation between BPTT and 3F learning rules [6], [11], [33], is discussed.

A. Spiking Neural Networks (SNNs)

Among all the mathematical models to describe the neuronal dynamics of biological neurons, the LIF model has been extensively used for machine learning tasks. One of the main reasons for this is that the LIF model is described by simple discrete recurrent equations that can be implemented efficiently while still capturing the most essential features of biological spiking neurons. The LIF model can be mathematically represented as follows:

$$u_i[t] = \gamma(u_i[t-1] - r_i[t-1]) + w_{ij}^{\text{ff}}x_j[t] + w_{ik}^{\text{rec}}y_k[t-1] \quad (1)$$

$$y_i[t] = \Theta(u_i[t] - v_{th}) \quad (2)$$

$$r_i[t] = \begin{cases} v_{th}y_i[t] & \text{for soft reset} \\ u_i[t]y_i[t] & \text{for hard reset} \end{cases} \quad (3)$$

Where u_i represents the membrane potential of the i -th neuron, w_{ij}^{ff} is the forward synaptic strength between the i -th post-synaptic neuron and the j -th pre-synaptic neuron, and w_{ik}^{rec} is the synaptic strength between the i -th and k -th neurons in the same layer. Moreover, γ is the leak factor that reduces the membrane potential over time, v_{th} is the threshold voltage, and Θ is the Heaviside function. So when u_i reaches the v_{th} , the neuron and output binary spike or action potential (y_i). Such action potential triggers the reset mechanism, represented by the reset signal r_i , which reduces the magnitude of u_i .

B. Synaptic Time-Dependent Plasticity (STDP)

STDP is a learning mechanism observed in various neural systems, from invertebrates to mammals, and is believed to play a critical role in the formation and modification of neural connections in the brain in processes such as learning and memory [4]. STDP describes how the synaptic strength (w_{ij}) between two neurons can change based on the temporal order of their spiking activity. Specifically, STDP describes the phenomenon by which w_{ij} is potentiated if the pre-synaptic neuron fires just before the post-synaptic neuron fires, and w_{ij} is depressed if the pre-synaptic neuron fires just after the post-synaptic neuron fires. This means that STDP rewards causality and punishes non-causality. However, [34] suggests that STDP favoring causality can be a transitory effect, and over time, STDP evolves to reward both causal and non-causal relations in favor of synchrony. Such general dynamics of STDP can be described by the following equation:

$$\Phi(t_i, t_j) = \begin{cases} \alpha_{pre} \lambda_{pre}^{t_i - t_j} & \text{if } t_i \geq t_j \text{ (causal)} \\ \alpha_{post} \lambda_{post}^{t_j - t_i} & \text{if } t_i < t_j \text{ (non-causal)} \end{cases} \quad (4)$$

Where $\Phi(t_i, t_j)$ represents the magnitude of the change in the synaptic strength (Δw_{ij}), t_i and t_j represent the firing times of the post- and pre-synaptic neurons, α_{pre} and λ_{pre} are strength and exponential decay factor of the causal term, respectively. Similarly, α_{post} and λ_{post} parameterize the anti-causal effect. The effects of each parameter are visualized in Fig. 2. Note that when $\alpha_{post} < 0$, STDP favors causality while $\alpha_{post} > 0$, STDP favors synchrony.

Based on STDP, the change of the synaptic strengths at time t can be computed using local variables by the following learning rule [4]:

$$\Delta w_{ij}[t] = \sum_{t'=0}^t \Phi(t, t') y_i[t] x_j[t'] + \sum_{t'=0}^{t-1} \Phi(t', t) y_i[t'] x_j[t] \quad (5)$$

$$w_{ij}[t+1] = w_{ij}[t] + \Delta w_{ij}[t] \quad (6)$$

Where y_i and y_j are binary values representing the post- and pre-synaptic activity, respectively.

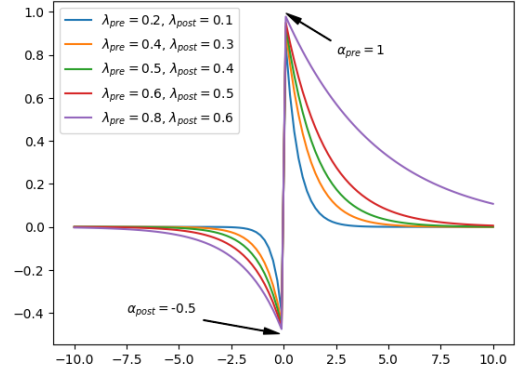


Fig. 2. Representation of the parametric equation for the STDP mechanism favoring causality (4). The x-axis represents the time difference between the occurrence of pre-synaptic activity (t_i) and post-synaptic activity (t_j). While the y-axis represents the magnitude of change in the synaptic strength.

C. BPTT and 3F learning rules

Backpropagation Through Time (BPTT) is the algorithm by default used to train spiking neural networks (SNNs) as it is able to solve spatial and temporal credit assignment problems. BPTT calculates the gradients by unfolding all layers of the network in time and applying the chain rule to compute the gradient as:

$$\frac{\partial \mathcal{L}}{\partial \mathbf{w}} = \sum_t^T \frac{\partial \mathcal{L}[t]}{\partial \mathbf{y}[t]} \frac{\partial \mathbf{y}[t]}{\partial \mathbf{u}[t]} \frac{\partial \mathbf{u}[t]}{\partial \mathbf{w}} \quad (7)$$

Although BPTT can yield satisfactory outcomes, its computational requirements scale with time, posing a limitation. Moreover, it is widely acknowledged that BPTT is not a biologically plausible method, as highlighted in [35].

In contrast, three-factor (3F) learning rules [19] are a more bio-plausible method that uses the combination of inputs, outputs, and a global learning signal to compute the synaptic plasticity. The general idea of the 3F rules is based on that synapses are updated only if a signal called eligibility trace e_{ij} is present. This eligibility trace is computed based on a general function of the pre- and post-synaptic activity decaying over time. Such behavior is modeled on the following recurrent equation:

$$e_{ij}[t] = \beta e_{ij}[t-1] + f(y_i[t])g(x_j[t]) \quad (8)$$

Where β is an exponential decay factor, $f(y_i[t])$ is a function of the post-synaptic activity, and $g(x_j[t])$ is a function of the pre-synaptic activity. Then, the change of the synaptic strengths (w_{ij}) is obtained by modulating e_{ij} with a global learning signal (δ_i) as:

$$\Delta w_{ij} = \sum_t \delta_i[t] e_{ij}[t] \quad (9)$$

3F learning rules have demonstrated their effectiveness in training SNNs, as shown in [11]. Additionally, it is possible to approximate BPTT using a 3F rule when the learning signal ($\delta_i[t]$) is computed as $\frac{\partial \mathcal{L}[t]}{\partial \mathbf{y}[t]}$, and the eligibility trace approximates $\frac{\partial \mathbf{y}[t]}{\partial \mathbf{u}[t]} \frac{\partial \mathbf{u}[t]}{\partial \mathbf{w}}$, as discussed in [11], [33]. However, it is important to note that 3F rules formulated as (8) exhibit

a memory complexity of $O(n^2)$, rendering them impractical for deep SNNs.

IV. STDP-INSPIRED TEMPORAL LOCAL LEARNING RULE (S-TLLR)

A. Overview of S-TLLR and its key features

We propose a novel three-factor learning rule, S-TLLR, which is inspired by the STDP mechanism discussed in Section III-B. The key features of S-TLLR are as follows: temporally local learning rule, leverage the non-causal relation of the spiking activity and present a linear memory complexity with the number of neurons.

The temporal locality of S-TLLR comes from its formulation as a three-factor learning rule 9. By computing and keeping track of an evolving eligibility trace (e_{ij}) based on previous neural activity, it is possible to store the essential information required to perform neural plasticity without having to store every single previous state. Specifically, we compute e_{ij} as a linear combination of pre- and post-synaptic activity and a low-pass filtered version of both of them. Since all the variables involved in the computation of e_{ij} can be computed forward in time, our method is temporally local.

Regarding memory complexity, the conventional computation of an eligibility trace involves a recurrent equation as described in 8. In such formulation, the eligibility trace is a state requiring a memory that scales linearly with the number of synapses ($O(n^2)$) instead of the number of neurons. For the S-TLLR, we dropped the recurrent term and considered only the instantaneous term in 8 to compute the eligibility trace. The instantaneous eligibility trace can be computed based on states of pre and post-synaptic activity that require memory scaling linearly with the number of neurons ($O(n)$). This low-memory complexity is a key aspect of S-TLLR since it enables the method to be used in deep neural models where methods such as [11]–[15] are impractical.

Finally, since BPTT is based on the propagation of errors in time, it only uses causal relations to compute gradients, that is, the relation between an output $y[t]$ and inputs $x[t], x[t-1], \dots, x[0]$. BPTT leverages only causal information as shown in Fig. 1a (red dotted line). Also, methods derived from BPTT such as [11]–[16] use exclusively causal relations. We took inspiration from the STDP mechanisms, which use both causal and non-causal information (Fig. 1b, red and blue dotted lines), to formulate S-TLLR as a three-factor learning rule with a learning signal modulating instantaneous eligibility trace signal as shown in Fig. 1c. Later in Section V, we show that considering such non-causal relations in the learning process leads to better task performance.

B. Technical details and implementation of S-TLLR

As discussed in the previous section, our proposed method, S-TLLR has the form of a three-factor learning rule, $\Delta w_{ij} = \sum_T L_i[t] e_{ij}[t]$, involving a global learning signal $L_i[t]$ and an eligibility trace, $e_{ij}[t]$, computed based on the pre- and post-synaptic activity. To reduce the square memory complexity of the eligibility trace as described in 9, we omit the recurrent term ($\lambda e_{ij}[t-1]$) and focus only on the instantaneous term. In

this way, the memory complexity of our method is linear with the number of neurons ($O(n)$) instead of a square. Moreover, we compute the instantaneous term based on a generalized version of the STDP equation described in (5) that can use a secondary activation function instead of the Heaviside function. In other words, the instantaneous eligibility trace is computed as follows after factorizing and replacing (4) in (5):

$$e_{ij}[t] = \Psi(u_i[t]) \sum_{t'=0}^t \alpha_{pre} \lambda_{pre}^{t-t'} x_j[t'] + x_j[t] \sum_{t'=0}^{t-1} \alpha_{post} \lambda_{post}^{t-t'} \Psi(u_i[t']) \quad (10)$$

Here, Ψ is a secondary activation function that can be different from the firing function used in (2). This gives the plasticity rule an extra degree of flexibility. Note that (10) can be computed forward in time and using only information locally available to the neuron. Furthermore, (10) considers both causal (first term on the right side) and non-causal (second term) relations that are not captured in BPTT or its approximations [11], [12], [16]. The causal relations are captured as the correlation between the current post-synaptic activity and the low-pass filtered pre-synaptic activity. Conversely, the non-causal relations are captured as the correlation of the current pre-synaptic activity and the low-pass filtered post-synaptic activity.

The complete plasticity rule uses a global learning signal ($\delta_i[t]$) to modulate $e_{ij}[t]$ in order to update the synaptic connections as follows:

$$w_{ij} := w_{ij} + \rho \sum_{t=T_l}^T \delta_i[t] e_{ij}[t] \quad (11)$$

where ρ is the learning rate, T is the total number of time steps for the forward pass, and T_l is the initial time step for which the learning signal is available. Depending on the task, good performance can be achieved even if the learning signal is available just for the last time step ($T_l = T$).

Moreover, $\delta_i[t]$ is computed as the instantaneous error backpropagated from the top layer (L) to the layer (l) as:

$$\delta_i^{(l)}[t] = \frac{\partial \mathcal{L}(\mathbf{y}^L[t], \mathbf{y}^*)}{\partial y_i^{(l)}[t]} \quad (12)$$

Where \mathbf{y}^* is the ground truth label vector, $\mathbf{y}^L[t]$ is the instantaneous output vector of layer L , and \mathcal{L} is the loss function. Note that the backpropagation occurs through the layers and not in time, so the S-TLLR is temporally local.

Using random feedback connections to produce the learning signal is also possible. In such case, the S-TLLR become spatially local as well. In particular, we explore the direct feedback alignment (DFA) [20] method to produce the learning signal for audio classification and gesture recognition, which is later discussed in Section V. Although such experiments give us competitive results, it is well known that DFA and its variants do not scale well with deeper networks. Hence, in most of our experiments, we used error-backpropagation through the layer to produce the learning signal.

The complete algorithm for a multilayer implementation is described in Algorithm 1.

Algorithm 1 S-TLLR algorithm

Require: $x, \mathbf{y}^*, \mathbf{w}, T, T_l, \rho$

- 1: Initialize $\delta^L = \nabla_{\mathbf{y}^L[t]} \mathcal{L}(\mathbf{y}^L[t], \mathbf{y}^*)$
- 2: **for** $t = 1, 2, \dots, T$ **do**
- 3: **for** $l = 1, 2, \dots, L$ **do**
- 4: Update membrane potential $\mathbf{u}^{(l)}[t]$ with (1)
- 5: Produce output spikes $\mathbf{y}^{(l)}[t]$ with (2)
- 6: Update eligibility trace $\mathbf{e}^{(l)}[t]$ with (10)
- 7: **end for**
- 8: **if** $t \geq T_l$ **then**
- 9: Compute $\Delta \mathbf{w}[t]$ with Algorithm 2
- 10: **end if**
- 11: **end for**
- 12: **for** $l = 1, 2, \dots, L$ **do**
- 13: Update weights $\mathbf{w}^{(l)} := \mathbf{w}^{(l)} + \rho \sum_T \Delta \mathbf{w}^{(l)}[t]$
- 14: **end for**
- 15: **return** \mathbf{w}

Algorithm 2 S-TLLR algorithm - learning signal generation

Require: $x, \mathbf{y}, \mathbf{y}^*, \mathbf{w}, \mathbf{u}, t$

- 1: Initialize $\delta^L = \nabla_{\mathbf{y}^L[t]} \mathcal{L}(\mathbf{y}^L[t], \mathbf{y}^*)$
- 2: Initialize $\mathbf{a}^{(L)} := \mathbf{1}$
- 3: **for** $l = L - 1, L - 2, \dots, 2$ **do**
- 4: **if** learning signal produced by backpropagation **then**
- 5: $\delta^{(l)} = \mathbf{a}^{(l+1)} \odot (\mathbf{w}^{(l+1)\top} \delta^{(l+1)})$
- 6: $\mathbf{a}^{(l)} = \delta^{(l)} \odot \Theta'(\mathbf{u}^{(l)}[t])$ $\{\Theta'$ is a surrogate gradient $\}$
- 7: **else if** learning signal produced by random feedback **then**
- 8: $\delta^{(l)} = \mathbf{B}^{(l)} \delta^{(L)}$ $\{\mathbf{B}^{(l)}$ is a fixed random matrix $\}$
- 9: **end if**
- 10: **end for**
- 11: $\Delta w_{ij}^{(L)}[t] = \delta_i^L y_j^{(L-1)}[t]$ $\{\text{Last layer}\}$
- 12: $\Delta w_{ij}^{(l)}[t] = \delta_i^{(l)} e_{ij}^{(l-1)}[t]$ $\{\text{Hidden layers}\}$
- 13: **return** $\Delta \mathbf{w}[t]$

V. EXPERIMENTAL EVALUATION

This section describes the experimental evaluation performed with S-TLLR. We extensively evaluated S-TLLR on several benchmark event-based datasets. First, we describe the dataset pre-processing, network architectures, and loss functions used for each task. Following that, we describe the effect of causal and non-causal relations on learning. Finally, the performance obtained with S-TLLR is compared with a baseline based on BPTT and some previous works.

A. Datasets and experimental setup

We conducted experiments on event-based datasets, such as DVS128 Gesture [36], DVS CIFAR-10 [37], SHD [28] and MVSEC [38], covering a range of applications such as image and gesture recognition, audio classification, and optical flow estimation.

1) *Network architectures:* For experiments on image and gesture recognition, we use a VGG-9 model with the following structure: 64C3-128C3-MP2S2-256C3-256C3-MP2S2-512C3-512C3-MP2S2-512C3-512C3-AP2S2-FC, where we use the notation 64C3 for a convolutional layer with 64 output channels and a kernel size of 3, MP2S2 and AP2S2 for max and average pooling layer with a kernel size of 2 with a stride of 2, and FC for a fully connected layer. In addition, instead of batch normalization, we use weight standardization [39] similar to [16]. Also, the leak factor and threshold are $\gamma = 0.5$ and $v_{th} = 0.8$, respectively.

For experiments with the SHD dataset, we use a recurrent SNN (RSNN) with one recurrent layer of 450 neurons and one leaky integrator layer with 20 neurons as a readout layer, similar to [14], [15]. Both layers have a leak factor $\gamma = 0.99$, and the recurrent LIF layer uses $v_{th} = 0.8$.

We use Fully-Spiking FlowNet (FSFN) for optical flow estimation, proposed in [40]. Such FSFN is a U-Net-like architecture with the main feature of performing only binary spike computation in all its layers. The main difference with respect to the FSFN on [40] is that we use weight standardization [39] for all the convolutional layers. In addition, we train the model using ten time steps without encoding temporal information on the input, in contrast to [40] that uses the encoding method proposed in [41]. Also, the leak factor and threshold of the LIF neurons used for our FSFN are 0.88 and 0.6, respectively.

2) *Data pre-processing:* Here we describe the data pre-processing for each dataset:

- DVS Gesture: the recordings were split into sequences of 1.5 seconds of duration, and the events were accumulated into 20 bins, with each bin having a 75 ms time window. Then, the event frames were resized to a size of 32×32 , while maintaining the positive and negative polarities as channels.
- DVS CIFAR10: the recordings were wrapped into ten bins with the same time window size for each bin. Then, the event frames were resized to a dimension of 48×48 . Additionally, a random crop with a padding of 4 was used for data augmentation.
- SHD: the events in each sequence were wrapped into 100 bins, each with a time window duration of 10 ms. No data augmentations techniques were used for SHD.
- MVSEC: the events between two consecutive grayscale frames were wrapped into ten bins, keeping the negative and positive polarities as channels. Then, the event frames are fed to the SNN model sequentially.

3) *Loss functions:* For image, gesture, and audio classification, we used cross-entropy (CE) loss and computed the learning signal with (12) using the ground truth labels (\mathbf{y}^*). In contrast, for optical flow, we used the self-supervised loss based on the photometric and smooth loss as described in Equation (5) at [41].

Furthermore, in the context of image and gesture recognition, the learning signal (δ) is exclusively generated for the final five time steps ($T_l = 5$). On the other hand, for audio classification, we employ $T_l = 90$, while for optical flow, we employ $T_l = 1$. This results in a reduction in the number

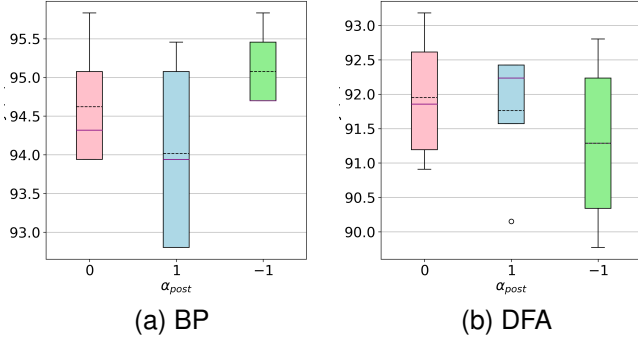


Fig. 3. Experiments on the DVS Gesture dataset with a VGG-9 architecture. First, the effects of including non-causal terms in the computation of the eligibility trace with the following STDP parameters constant $(\lambda_{post}, \lambda_{pre}, \alpha_{pre}) = (0.2, 0.75, 1)$ when the learning signal (δ) is generated using (a) backpropagation (BP), and (b) direct feedback alignment (DFA). (c) Effects of using a decaying factor from the leak spiking parameter ($\gamma = 0.5$) to compute the causal term on the eligibility trace, with the following parameters constant $(\lambda_{post}, \alpha_{post}, \alpha_{pre}) = (0.2, -1, 1)$ with the learning signal produce with BP. The horizontal solid purple line indicates the median value, and the dashed black line indicates the mean value over five trials.

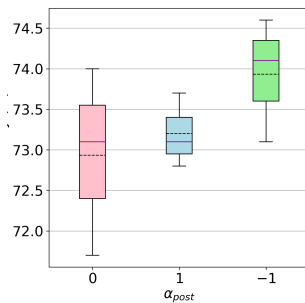


Fig. 4. Experiments on the DVS CIFAR10 dataset with a VGG-9 architecture generating the learning signal (δ) with backpropagation. The effects of including non-causal terms in the computation of the eligibility trace with the following STDP parameters constant $(\lambda_{post}, \lambda_{pre}, \alpha_{pre}) = (0.2, 0.5, 1)$

of computations compared to BPTT of $4\times$, $1.1\times$, and $10\times$ respectively.

B. Effects of causality and non-causality on learning

We performed ablation studies on the DVS Gesture, DVS CIFAR10, and SHD datasets to evaluate the effect of

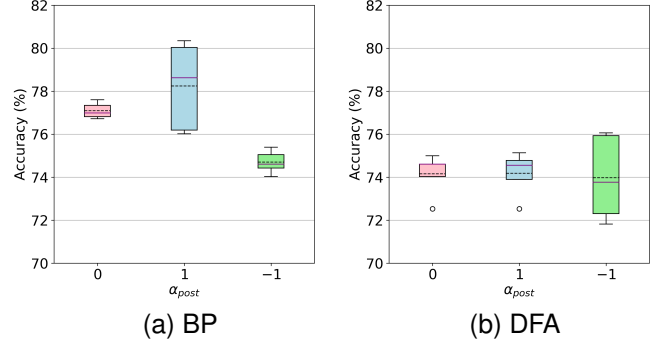


Fig. 5. Effect of the non-causality term on the performance of an RSNN with the SHD dataset when the learning signal is produced using (a) backpropagation of errors through layers and (b) direct feedback alignment (DFA). For all the experiments, the following STDP parameters are constant $(\lambda_{post}, \lambda_{pre}, \alpha_{pre}) = (0.5, 1, 1)$, and only the α_{post} parameter change. For $\alpha_{post} = 0$ only the causal terms are considered when computing the eligibility trace, $\alpha_{post} = 1$ corresponds to the non-causal term being added positively to the causal terms and $\alpha_{post} = -1$ corresponds to the non-causal term being penalized. The plots were computed based on five trials. The solid purple line indicates the median value, and the dashed black line indicates the mean value.

the STDP parameters $(\lambda_{post}, \lambda_{pre}, \alpha_{post}, \alpha_{pre})$ on the learning process.

First, we evaluate the effect of adding a non-causal term in the computation of the instantaneous eligibility trace (10). For this purpose, we train the VGG9 model five times with the same random seeds for 30 epochs and 300 epochs in the DVS Gesture and DVS CIFAR10 datasets, respectively. Similarly, the RSNN model was trained five times during 200 epochs on the SHD. To measure the effect of the non-causal term, we change the α_{post} factor. When $\alpha_{post} = 0$, only causal terms are considered, while $\alpha_{post} = 1$ ($\alpha_{post} = -1$) means that the non-causal term is added positively (negatively) on (10). Firstly, we use BP to produce the learning signal. As shown in Fig. 3a and Fig. 4, for gesture and image recognition, it can be seen that using $\alpha_{post} = -1$ improves the average accuracy performance of the model with respect to only using causal terms $\alpha_{post} = 0$. In contrast, for SHD, using $\alpha_{post} = 1$ improves the average performance over using only causal terms, as shown in Fig. 5a. However, when the learning signal is produced by using random feedback via direct feedback alignment (DFA), there is no significant difference between including non-causal terms or not. For instance, the average performance of the RSNN model using $\alpha_{post} = 1$ is still better, but for a small margin, as shown in Fig. 5b. And, for the VGG9 model, $\alpha_{post} = 1$ and $\alpha_{post} = 0$ performance similarly and better than $\alpha_{post} = -1$, as shown in Fig. 3b. This could indicate that a more precise learning signal, such as BP, is required to take advantage of the non-causal terms.

Moreover, since the eligibility trace in S-TLLR is described as a parametric equation (10), there is room for further exploring the parameters that could improve the model's performance. Particularly, we focused on the λ_{pre} term that controls the decay factor of the input trace. For works attempting to approximate BPTT [11], [12], [16], such λ_{pre} is equal to the leak factor (γ) of the spiking neurons during the forward pass.

However, as shown in Fig. 3c, using a λ_{pre} slightly higher than γ can result in improving the average accuracy performance of the model.

C. Performance comparison

This section compares the performance obtained by an SNN model trained with S-TLLR and BPTT. For fair comparison, we used the same random initialization, parameters, and hyperparameters in all the experiments on the same task. While we mainly compared our results with BPTT, results from previous works are included for context.

1) *Image and Gesture Recognition*: We train the VGG-9 model, described in Section V-A1, for 300 epochs using the Adam optimizer with a learning rate of 0.001 on both DVS Gesture and DVS CIFAR10 datasets. The models were trained five times using five different random seeds. The baseline was set using BPTT, while the models trained using S-TLLR used the following STDP parameters: $(\lambda_{post}, \lambda_{pre}, \alpha_{post}, \alpha_{pre}) = (0.2, 0.75, -1, 1)$ for DVS Gesture and $(\lambda_{post}, \lambda_{pre}, \alpha_{post}, \alpha_{pre}) = (0.2, 0.5, -1, 1)$ for DVS CIFAR10.

The results of the training are shown in Table II. In both tasks, S-TLLR shows a competitive performance compared to BPTT. In fact, for DVS Gesture, S-TLLR outperforms the average accuracy obtained by the baseline trained with BPTT. Because of the small size of the DVS Gesture dataset, and the complexity of the BPTT algorithm, the model overfits quickly resulting in lower performance. In contrast, S-TLLR avoids such overfitting effect due to its simple formulation and by updating the weights only on the last five timesteps. Table II also includes results from previous works using spiking models on the same datasets. For DVS Gesture, it can be seen that S-TLLR outperforms previous methods such as [16], [42], [43], in some cases with significantly less number of time-steps. In contrast, for DVS CIFAR10, S-TLLR outperforms the result from [44] that uses a deeper network, but is behind others such as [16], [45]. With respect to [45], S-TLLR is just behind by 0.9% while using half the number of time steps and a simpler spiking neuron model. Nevertheless, the disparity grows in comparison to [16]. This last comparison holds significant relevance due to the employment of a learning rule in [16] that shares similar memory and time complexity with S-TLLR. It is important to note, however, that while [16] calculates the learning signal for all 20 time steps, we solely compute it for the last five, effectively reducing the computational workload by a factor of four.

2) *Audio Classification*: As discussed previously in Section V-B, we found that adding a positive non-causal term ($\alpha_{post} = 1$) into the eligibility trace computation improves the average performance of an RSNN on the SHD dataset using both BP and DFA to generate the learning signal. One potential explanation for this observation is that setting $\alpha_{post} = 1$ reinforces the direction of gradient descent, resulting in faster convergence of the learning process. Furthermore, as detailed in Section III-B, the choice of $\alpha_{post} = 1$ promotes synchrony between inputs and outputs. This effect can be particularly advantageous in models with explicit recurrent connections,

TABLE II
COMPARISON OF ACCURACY PERFORMANCE ON THE DVS CIFAR10 AND DVS GESTURE DATASETS

Method	Model	Time-steps	Accuracy (Mean±Std)
DVS CIFAR10			
BPTT [44]	ResNet-19	10	67.8%
BPTT [46]	PLIF (7 layers)	20	74.8%
OTTT _A [16]	VGG-9	10	76.27 ± 0.05%
BPTT (baseline)	VGG-9	10	75.44 ± 0.76%
S-TLLR (Ours)	VGG-9	10	73.93 ± 0.62%
DVS128 Gesture			
SLAYER [42]	SNN (8 layers)	300	93.64 ± 0.49%
DECOLLE [43]	SNN (4 layers)	1800	95.54 ± 0.16%
OTTT _A [16]	VGG-9	20	96.88%
BPTT (baseline)	VGG-9	20	95.58 ± 1.08%
S-TLLR (Ours)	VGG-9	20	97.72 ± 0.38%

such as the RSNN architecture, compared to models with only implicit recurrency

In order to set a baseline, we train the same RSNN with the same hyperparameters using BPTT for five trials. As shown in Table III, the model trained with S-TLLR outperforms the baseline trained with BPTT. This result shows the capability of S-TLLR to achieve high performance and generalization. One reason why the baseline does not perform well, as suggested in [28], is that RSNN trained with BPTT quickly overfit. This also highlights a nice property of S-TLLR. Since it has a simpler formulation than BPTT, it can avoid overfitting, resulting in a better generalization. However, note that works such as [28], [45] can achieve better performance after carefully selecting the hyperparameters and using data augmentation techniques. In comparison with such works, our method still shows a competitive performance with the advantage of having a better memory complexity and a reduction of the number of computations of $1.1 \times$.

Furthermore, we compared our results with [14], [15], which uses the same RSNN network structure with LIF and ALIF (LIF with adaptative threshold) neurons and temporal local learning rules. Table III shows that using S-TLLR with BP for the learning signal results in better performance than those obtained with other temporal local learning rules, with the advantage of having a linear memory complexity instead of squared. Moreover, using DFA to generate the learning signal results in competitive performance with the advantage of being local in both time and space.

3) *Event-based Optical Flow*: The optical flow estimation is evaluated using the average endpoint error (AEE) metric that measures the Euclidean distance between the predicted flow (\mathbf{y}^{pred}) and ground truth flow (\mathbf{y}^{gt}) per pixel. For consistency, this metric is computed only for pixels containing events (P), similar to [40], [41], [47]–[49], given by the following expression:

$$\text{AEE} = \frac{1}{P} \sum_P \|\mathbf{y}_{i,j}^{\text{pred}} - \mathbf{y}_{i,j}^{\text{gt}}\|_2 \quad (13)$$

Where P is the set of all the pixels with events.

TABLE III
COMPARISON OF THE PERFORMANCE OF AN RSNN WITH ONE HIDDEN LAYER ON AUDIO CLASSIFICATION USING THE SHD DATASET

Method	Model	Memory Complexity	Accuracy (Mean±Std)
ETLP [14]	ALIF-RSNN	n^2	$74.59 \pm 0.44\%$
OSTTP [15]	LIF-RSNN	n^2	$77.33 \pm 0.8\%$
BPTT [45]	LIF-RSNN	Tn	83.41
BPTT [28]	LIF-RSNN	Tn	83.2 ± 1.3
BPTT (baseline)	LIF-RSNN	Tn	70.57 ± 0.96
S-TLLR_{BP} (Ours)	LIF-RSNN	n	$78.24 \pm 1.84\%$
S-TLLR_{DFA} (Ours)	LIF-RSNN	n	$74.60 \pm 0.52\%$

For this experiment, we trained the FSFN model, discussed in Section V-A1, with S-TLLR using the following STDP parameters $(\lambda_{post}, \lambda_{pre}, \alpha_{pre}) = (0.5, 0.8, 1)$ and $\alpha_{post} = [-0.2, 0.2, 0]$. The models were trained during 100 epochs using the Adam optimizer with a learning rate of 0.0002, a batch size of 8, and with the learning signal obtained from the photometric loss just for the last time step ($T_l = 1$). As it is shown in Table IV, the FSFN model trained using S-TLLR with $\alpha_{post} = -0.2$ shows a performance close to the baseline implementation trained with BPTT. Although we mainly compared our model with BPTT, to take things into perspective, we include results from other previous works. Among the spiking models, our model trained with S-TLLR has the second-best average performance (AEE sum) in comparison with such spiking models of similar architecture and size trained with BPTT [40], [47], [50]. Moreover, it also presents better average performance than hybrid networks, analog recurrent, and analog models [27], [41], [48] trained with BPTT and BP.

The results indicate that our method achieves high performance on a complex spatio-temporal task, such as optical flow estimation, with a $10\times$ reduction in the number of computations by just updating the model in the last time step. Moreover, since our method is time-independent, it enables the possibility of doing online learning and learning with longer sequences while maintaining constant computational resources.

VI. CONCLUSION

In this work, we proposed S-TLLR, a novel temporal local learning rule inspired by the STDP mechanism, for training deep spiking neural networks on event-based datasets. Our proposed learning rule, S-TLLR, can achieve competitive performance in comparison to BPTT on several event-based datasets with the advantage of having a constant memory requirement. In contrast to BPTT (or other temporal learning rules) with memory requirements scaling with the number of time steps and neurons ($O(Tn)$ or $O(n^2)$), S-TLLR memory is just proportional to the number of neurons ($O(n)$). Moreover, in contrast with previous works that are derived from BPTT as approximations, and therefore using only causal relations between inputs and outputs, S-TLLR explores a different direction by leveraging causal and non-causal relations based

on a generalized parametric STDP equation. We have experimentally demonstrated on several event-based datasets that including such non-causal relations can improve the SNN performance in comparison with temporal local learning rules using just causal relations. Also, we could observe that tasks where spatial information is predominant, such as DVS CIFAR-10, DVS Gesture, and MVSEC, benefit from causality. In contrast, in a task like SHD, where temporal information is predominant, benefits from synchrony ($\alpha_{post} = 1$), rewarding both causal and non-causal. Moreover, by computing the learning signal just for a portion of the total time steps, S-TLLR reduces the number of computations in the range of $1.1\times$ to $10\times$. In summary, S-TLLR can achieve high performance while being memory-efficient and requiring only information locally in time, therefore enabling online updates. Moreover, since S-TLLR uses both causal and non-causal information through a parametric formulation, such parameters can be further fine-tuned or meta-learned to achieve better performance.

ACKNOWLEDGMENTS

This work was supported in part by the Center for Brain-Inspired Computing (C-BRIC), one of six centers in JUMP, funded by Semiconductor Research Corporation (SRC) and DARPA, the Micro4AI program from IARPA, National Science Foundation, and Intel Corporation.

REFERENCES

- [1] T. B. Brown, B. Mann, N. Ryder, M. Subbiah, J. Kaplan, P. Dhariwal, A. Neelakantan, P. Shyam, G. Sastry, A. Askell, S. Agarwal, A. Herbert-Voss, G. Krueger, T. Henighan, R. Child, A. Ramesh, D. M. Ziegler, J. Wu, C. Winter, C. Hesse, M. Chen, E. Sigler, M. Litwin, S. Gray, B. Chess, J. Clark, C. Berner, S. McCandlish, A. Radford, I. Sutskever, and D. Amodei, "Language Models are Few-Shot Learners," in *Advances in Neural Information Processing Systems*, 2020, pp. 1877–1901.
- [2] A. Dosovitskiy, L. Beyer, A. Kolesnikov, D. Weissenborn, X. Zhai, T. Unterthiner, M. Dehghani, M. Minderer, G. Heigold, S. Gelly, J. Uszkoreit, and N. Houlsby, "An Image is Worth 16x16 Words: Transformers for Image Recognition at Scale," in *International Conference on Learning Representations*, 2021.
- [3] K. Roy, A. Jaiswal, and P. Panda, "Towards spike-based machine intelligence with neuromorphic computing," *Nature*, vol. 575, no. 7784, pp. 607–617, 11 2019. [Online]. Available: <http://www.nature.com/articles/s41586-019-1677-2>
- [4] W. Gerstner, W. M. Kistler, R. Naud, and L. Paninski, *Neuronal Dynamics*. Cambridge: Cambridge University Press, 7 2014. [Online]. Available: <https://www.cambridge.org/core/product/identifier/9781107447615/type/book>
- [5] D. V. Christensen, R. Dittmann, B. Linares-Barranco, A. Sebastian, M. Le Gallo, A. Redaelli, S. Slesazcek, T. Mikolajick, S. Spiga, S. Menzel, I. Valov, G. Milano, C. Ricciardi, S.-J. Liang, F. Miao, M. Lanza, T. J. Quill, S. T. Keene, A. Salleo, J. Grollier, D. Marković, A. Mizrahi, P. Yao, J. J. Yang, G. Indiveri, J. P. Strachan, S. Datta, E. Vianello, A. Valentian, J. Feldmann, X. Li, W. H. P. Pernice, H. Bhaskaran, S. Furber, E. Neftci, F. Scherr, W. Maass, S. Ramaswamy, J. Tapsen, P. Panda, Y. Kim, G. Tanaka, S. Thorpe, C. Bartolozzi, T. A. Cleland, C. Posch, S. Liu, G. Panuccio, M. Mahmud, A. N. Mazumder, M. Hosseini, T. Mohsenin, E. Donati, S. Tolu, R. Galeazzi, M. E. Christensen, S. Holm, D. Ielmini, and N. Pridys, "2022 roadmap on neuromorphic computing and engineering," *Neuromorphic Computing and Engineering*, vol. 2, no. 2, p. 022501, 6 2022.
- [6] J. K. Eshraghian, M. Ward, E. Neftci, X. Wang, G. Lenz, G. Dwivedi, M. Bennamoun, D. S. Jeong, and W. D. Lu, "Training Spiking Neural Networks Using Lessons From Deep Learning," 9 2021. [Online]. Available: <http://arxiv.org/abs/2109.12894>

TABLE IV
COMPARISON OF THE AVERAGE END-POINT ERROR (AEE) ON THE MVSEC [38] DATASET [AEE LOWER IS BETTER]

Models	Training Method	Type	Outdoor_day1 AEE	Indoor_flying1 AEE	Indoor_flying2 AEE	Indoor_flying3 AEE	AEE sum
FSFN$_{\alpha_{post} = -0.2}$ (Ours)	S-TLLR	Spiking	0.50	0.76	1.19	1.00	3.45
FSFN$_{\alpha_{post} = 0.2}$ (Ours)	S-TLLR	Spiking	0.54	0.78	1.28	1.09	3.69
FSFN$_{\alpha_{post} = 0}$ (Ours)	S-TLLR	Spiking	0.50	0.77	1.25	1.08	3.60
FSFN (baseline)	BPTT	Spiking	0.45	0.76	1.17	1.02	3.40
FSFN _{FP} [40]	BPTT	Spiking	0.51	0.82	1.21	1.07	3.61
Base-SNN [47]	BPTT	Spiking	0.44	0.79	1.37	1.11	3.78
XLIF-EV-FlowNet [50]	BPTT	Spiking	0.45	0.73	1.45	1.17	3.80
Spike-FlowNet [41]	BPTT	Hybrid	0.49	0.84	1.28	1.11	3.72
EV-FlowNet _{EW-DR} [27]	BPTT	Analog	0.92	0.79	1.40	1.18	4.29
EV-FlowNet [48]	BP	Analog	0.49	1.03	1.72	1.53	4.77
Zhu et al. [49]	BP	Analog	0.32	0.58	1.02	0.87	2.79
Zero prediction	-	-	1.08	1.29	2.13	1.88	6.38

- [7] M. Davies, N. Srinivasa, T. H. Lin, G. Chinya, Y. Cao, S. H. Choday, G. Dimou, P. Joshi, N. Imam, S. Jain, Y. Liao, C. K. Lin, A. Lines, R. Liu, D. Mathaikutty, S. McCoy, A. Paul, J. Tse, G. Venkataramanan, Y. H. Weng, A. Wild, Y. Yang, and H. Wang, "Loihi: A Neuromorphic Manycore Processor with On-Chip Learning," *IEEE Micro*, vol. 38, no. 1, pp. 82–99, 1 2018.
- [8] A. Sengupta, Y. Ye, R. Wang, C. Liu, and K. Roy, "Going Deeper in Spiking Neural Networks: VGG and Residual Architectures," *Frontiers in Neuroscience*, vol. 13, p. 95, 3 2019.
- [9] E. O. Neftci, H. Mostafa, and F. Zenke, "Surrogate Gradient Learning in Spiking Neural Networks: Bringing the Power of Gradient-based optimization to spiking neural networks," *IEEE Signal Processing Magazine*, vol. 36, no. 6, pp. 51–63, 11 2019.
- [10] W. Ponghiran and K. Roy, "Spiking Neural Networks with Improved Inherent Recurrence Dynamics for Sequential Learning," in *Proceedings of the AAAI Conference on Artificial Intelligence*, vol. 36, no. 7, 6 2022, pp. 8001–8008.
- [11] G. Bellec, F. Scherr, A. Subramoney, E. Hajek, D. Salaj, R. Legenstein, and W. Maass, "A solution to the learning dilemma for recurrent networks of spiking neurons," *Nature Communications*, vol. 11, no. 1, 12 2020.
- [12] T. Bohnstingl, S. Wozniak, A. Pantazi, and E. Eleftheriou, "Online Spatio-Temporal Learning in Deep Neural Networks," *IEEE Transactions on Neural Networks and Learning Systems*, 2022.
- [13] R. J. WILLIAMS and D. ZIPSER, "Experimental Analysis of the Real-time Recurrent Learning Algorithm," *Connection Science*, vol. 1, no. 1, pp. 87–111, 1 1989. [Online]. Available: <https://www.tandfonline.com/doi/full/10.1080/09540098908915631>
- [14] F. M. Quintana, F. Perez-Peña, P. L. Galindo, E. O. Neftci, E. Chicca, and L. Khacef, "ETLP: Event-based Three-factor Local Plasticity for online learning with neuromorphic hardware," 1 2023. [Online]. Available: <https://arxiv.org/abs/2301.08281v2>
- [15] T. Ortner, L. Pes, J. Gentinetta, C. Frenkel, and A. Pantazi, "Online Spatio-Temporal Learning with Target Projection," in *2023 IEEE 5th International Conference on Artificial Intelligence Circuits and Systems*, 4 2023. [Online]. Available: <https://arxiv.org/abs/2304.05124v2>
- [16] M. Xiao, Q. Meng, Z. Zhang, D. He, and Z. Lin, "Online Training Through Time for Spiking Neural Networks," in *36th Conference on Neural Information Processing Systems (NeurIPS 2022)*, 10 2022. [Online]. Available: <http://arxiv.org/abs/2210.04195>
- [17] G. Q. Bi and M. M. Poo, "Synaptic Modifications in Cultured Hippocampal Neurons: Dependence on Spike Timing, Synaptic Strength, and Postsynaptic Cell Type," *Journal of Neuroscience*, vol. 18, no. 24, pp. 10464–10472, 12 1998. [Online]. Available: <https://www.jneurosci.org/content/18/24/10464https://www.jneurosci.org/content/18/24/10464.abstract>
- [18] S. Song, K. D. Miller, and L. F. Abbott, "Competitive Hebbian learning through spike-timing-dependent synaptic plasticity," *Nature Neuroscience* 2000 3:9, vol. 3, no. 9, pp. 919–926, 9 2000. [Online]. Available: https://www.nature.com/articles/nn0900_919
- [19] W. Gerstner, M. Lehmann, V. Liakoni, D. Corneil, and J. Brea, "Eligibility Traces and Plasticity on Behavioral Time Scales: Experimental Support of NeoHebbian Three-Factor Learning Rules," *Frontiers in Neural Circuits*, vol. 12, 7 2018. [Online]. Available: <https://www.frontiersin.org/article/10.3389/fncir.2018.00053/full>
- [20] A. N. Trondheim, "Direct Feedback Alignment Provides Learning in Deep Neural Networks," *Advances in Neural Information Processing Systems*, vol. 29, 2016.
- [21] B. Rueckauer, I. A. Lungu, Y. Hu, M. Pfeiffer, and S. C. Liu, "Conversion of continuous-valued deep networks to efficient event-driven networks for image classification," *Frontiers in Neuroscience*, vol. 11, no. DEC, 12 2017.
- [22] P. U. Diehl and M. Cook, "Unsupervised learning of digit recognition using spike-timing-dependent plasticity," *Frontiers in Computational Neuroscience*, vol. 9, no. AUGUST, p. 99, 8 2015.
- [23] J. C. Thiele, O. Bichler, and A. Dupret, "Event-based, timescale invariant unsupervised online deep learning with STDP," *Frontiers in Computational Neuroscience*, vol. 12, p. 46, 6 2018.
- [24] S. R. Kheradpisheh, M. Ganjtabesh, S. J. Thorpe, and T. Masquelier, "STDP-based spiking deep convolutional neural networks for object recognition," *Neural Networks*, vol. 99, pp. 56–67, 3 2018.
- [25] N. Rathi and K. Roy, "DIET-SNN: A Low-Latency Spiking Neural Network With Direct Input Encoding and Leakage and Threshold Optimization," *IEEE Transactions on Neural Networks and Learning Systems*, pp. 1–9, 2021.
- [26] C. Lee, P. Panda, G. Srinivasan, and K. Roy, "Training deep spiking convolutional Neural Networks with STDP-based unsupervised pre-training followed by supervised fine-tuning," *Frontiers in Neuroscience*, vol. 12, no. AUG, p. 435, 8 2018.
- [27] F. Paredes-Vallés and G. C. de Croon, "Back to Event Basics: Self-Supervised Learning of Image Reconstruction for Event Cameras via Photometric Constancy," in *Proceedings of the IEEE Computer Society Conference on Computer Vision and Pattern Recognition*. IEEE Computer Society, 2021, pp. 3445–3454.
- [28] B. Cramer, Y. Stradmann, J. Schemmel, and F. Zenke, "The Heidelberg Spiking Data Sets for the Systematic Evaluation of Spiking Neural Networks," *IEEE Transactions on Neural Networks and Learning Systems*, vol. 33, no. 7, pp. 2744–2757, 7 2022.
- [29] W. Fang, Z. Yu, Y. Chen, T. Huang, T. Masquelier, and Y. Tian, "Deep Residual Learning in Spiking Neural Networks," in *Advances in Neural Information Processing Systems*, 2021, pp. 21 056–21 069.
- [30] A. Tavanaei and A. Maida, "BP-STDP: Approximating backpropagation using spike timing dependent plasticity," *Neurocomputing*, vol. 330, pp. 39–47, 2 2019.
- [31] Z. Hu, T. Wang, and X. Hu, "An STDP-Based Supervised Learning Algorithm for Spiking Neural Networks," in *Lecture Notes in Computer Science (including subseries Lecture Notes in Artificial Intelligence and Lecture Notes in Bioinformatics)*. Springer Verlag, 3 2017, vol. 10635 LNCS, pp. 92–100. [Online]. Available: http://link.springer.com/10.1007/978-3-319-70096-0_10
- [32] Y. Hao, X. Huang, M. Dong, and B. Xu, "A biologically plausible supervised learning method for spiking neural networks using the symmetric STDP rule," *Neural Networks*, vol. 121, pp. 387–395, 1 2020.

- [33] G. Martín-Sánchez, S. Bohté, and S. Otte, “A Taxonomy of Recurrent Learning Rules,” *Lecture Notes in Computer Science (including subseries Lecture Notes in Artificial Intelligence and Lecture Notes in Bioinformatics)*, vol. 13529 LNCS, pp. 478–490, 2022. [Online]. Available: https://link.springer.com/chapter/10.1007/978-3-031-15919-0_40
- [34] M. Anisimova, B. van Bommel, R. Wang, M. Mikhaylova, J. S. Wiegert, T. G. Oertner, and C. E. Gee, “Spike-timing-dependent plasticity rewards synchrony rather than causality,” *Cerebral Cortex*, vol. 33, no. 1, pp. 23–34, 12 2022. [Online]. Available: <https://academic.oup.com/cercor/article/33/1/23/6535691>
- [35] T. P. Lillicrap and A. Santoro, “Backpropagation through time and the brain,” *Current Opinion in Neurobiology*, vol. 55, pp. 82–89, 4 2019.
- [36] A. Amir, B. Taba, D. Berg, T. Melano, J. McKinstry, C. Di Nolfo, T. Nayak, A. Andreopoulos, G. Garreau, M. Mendoza, J. Kusnitz, M. Debole, S. Esser, T. Delbruck, M. Flickner, and D. Modha, “A Low Power, Fully Event-Based Gesture Recognition System,” in *2017 IEEE Conference on Computer Vision and Pattern Recognition (CVPR)*, vol. 2017-January. IEEE, 7 2017, pp. 7388–7397.
- [37] H. Li, H. Liu, X. Ji, G. Li, and L. Shi, “CIFAR10-DVS: An event-stream dataset for object classification,” *Frontiers in Neuroscience*, vol. 11, no. MAY, p. 309, 5 2017.
- [38] A. Z. Zhu, D. Thakur, T. Ozaslan, B. Pfrommer, V. Kumar, and K. Daniilidis, “The Multivehicle Stereo Event Camera Dataset: An Event Camera Dataset for 3D Perception,” *IEEE Robotics and Automation Letters*, vol. 3, no. 3, pp. 2032–2039, 7 2018.
- [39] S. Qiao, H. Wang, C. Liu, W. Shen, and A. Yuille, “Micro-Batch Training with Batch-Channel Normalization and Weight Standardization,” 3 2019. [Online]. Available: <https://arxiv.org/abs/1903.10520v2>
- [40] M. P. E. Apolinario, A. Kumar Kosta, U. Saxena, and K. Roy, “Hardware/Software co-design with ADC-Less In-memory Computing Hardware for Spiking Neural Networks,” 2022. [Online]. Available: <https://arxiv.org/abs/2211.02167>
- [41] C. Lee, A. K. Kosta, A. Z. Zhu, K. Chaney, K. Daniilidis, and K. Roy, “Spike-FlowNet: Event-Based Optical Flow Estimation with Energy-Efficient Hybrid Neural Networks,” in *European Conference on Computer Vision (ECCV)*, ser. Lecture Notes in Computer Science, vol. 12374, 2020, pp. 366–382.
- [42] S. B. Shrestha and G. Orchard, “SLAYER: Spike Layer Error Reassignment in Time,” *Advances in Neural Information Processing Systems*, vol. 31, 2018. [Online]. Available: <https://bitbucket.org/bamsmit/sl原因er>
- [43] J. Kaiser, H. Mostafa, and E. Neftci, “Synaptic Plasticity Dynamics for Deep Continuous Local Learning (DECOLLE),” *Frontiers in Neuroscience*, vol. 14, 5 2020.
- [44] H. Zheng, Y. Wu, L. Deng, Y. Hu, and G. Li, “Going Deeper With Directly-Trained Larger Spiking Neural Networks,” *Proceedings of the AAAI Conference on Artificial Intelligence*, vol. 35, no. 12, pp. 11 062–11 070, 5 2021. [Online]. Available: <https://ojs.aaai.org/index.php/AAAI/article/view/17320>
- [45] M. S. Bouanane, D. Cherifi, E. Chicca, and L. Khacef, “Impact of spiking neurons leakages and network recurrences on event-based spatio-temporal pattern recognition,” 11 2022. [Online]. Available: <https://arxiv.org/abs/2211.07761v1>
- [46] W. Fang, Z. Yu, Y. Chen, T. Masquelier, T. Huang, and Y. Tian, “Incorporating Learnable Membrane Time Constant To Enhance Learning of Spiking Neural Networks,” in *Proceedings of the IEEE/CVF International Conference on Computer Vision (ICCV)*, 2021, pp. 2661–2671. [Online]. Available: <https://github.com/fangw>
- [47] A. K. Kosta and K. Roy, “Adaptive-SpikeNet: Event-based Optical Flow Estimation using Spiking Neural Networks with Learnable Neuronal Dynamics,” 9 2022. [Online]. Available: <https://arxiv.org/abs/2209.11741v2>
- [48] A. Zhu, L. Yuan, K. Chaney, and K. Daniilidis, “EV-FlowNet: Self-Supervised Optical Flow Estimation for Event-based Cameras,” in *Robotics: Science and Systems XIV*. Robotics: Science and Systems Foundation, 6 2018, p. 62.
- [49] A. Z. Zhu, L. Yuan, K. Chaney, and K. Daniilidis, “Unsupervised event-based learning of optical flow, depth, and egomotion,” in *Proceedings of the IEEE Computer Society Conference on Computer Vision and Pattern Recognition*, vol. 2019-June. IEEE Computer Society, 6 2019, pp. 989–997.
- [50] J. J. Hagenaars, F. Paredes-Vallés, and G. C. H. E. De Croon, “Self-Supervised Learning of Event-Based Optical Flow with Spiking Neural Networks,” in *Advances in Neural Information Processing Systems*, 2021, pp. 7167–7179.



Marco P. E. Apolinario received his B.S. degree in Electronics Engineering at the National University of Engineering (UNI), Lima, Peru in 2017. Currently, he is pursuing his Ph.D. degree at Purdue University under the guidance of Prof. Kaushik Roy. His research focuses on the intersection of hardware-software co-design for brain-inspired computing, in-memory computing architectures, and energy-efficient learning algorithms for spiking neural networks.



Kaushik Roy is the Edward G. Tiedemann, Jr., Distinguished Professor of Electrical and Computer Engineering at Purdue University. He received his B.Tech from Indian Institute of Technology, Kharagpur, PhD from University of Illinois at Urbana-Champaign in 1990 and joined the Semiconductor Process and Design Center of Texas Instruments, Dallas, where he worked for three years on FPGA architecture development and low-power circuit design. His current research focuses on cognitive algorithms, circuits and architecture for energy-efficient neuromorphic computing/ machine learning, and neuro-mimetic devices. Kaushik has supervised more than 100 PhD dissertations and his students are well placed in universities and industry. He is the co-author of two books on Low Power CMOS VLSI Design (John Wiley & McGraw Hill).